J Biomol NMR (2015) 62:303–311
DOI 10.1007/s10858-015-9945-4

ARTICLE

Sequential backbone assignment based on dipolar amide-to-amide correlation experiments

ShengQi Xiang[1] · Kristof Grohe[1] · Petra Rovó[1] · Suresh Kumar Vasa[1] · Karin Giller[1] · Stefan Becker[1] · Rasmus Linser[1]

Received: 23 January 2015 / Accepted: 7 May 2015 / Published online: 15 May 2015

Abstract Proton detection in solid-state NMR has seen a tremendous increase in popularity in the last years. New experimental techniques allow to exploit protons as an additional source of information on structure, dynamics, and protein interactions with their surroundings. In addition, sensitivity is mostly improved and ambiguity in assignment experiments reduced. We show here that, in the solid state, sequential amide-to-amide correlations turn out to be an excellent, complementary way to exploit amide shifts for unambiguous backbone assignment. For a general assessment, we compare amide-to-amide experiments with the more common ^{13}C-shift-based methods. Exploiting efficient CP magnetization transfers rather than less efficient INEPT periods, our results suggest that the approach is very feasible for solid-state NMR.

Keywords Ultra-fast MAS · Proton-detected solid-state NMR · SH3 domain · Deuteration · Dipolar transfers

Introduction

Proton-detected solid-state NMR has become increasingly popular in the last years (Agarwal et al. 2014; Barbet-Massin et al. 2014; Bellstedt et al. 2012; Brown 2012; Knight et al. 2011; Linser et al. 2011a, b; Ma et al. 2014; Nishiyama et al. 2014; Xiang et al. 2014; Zhou et al. 2012). This is due to innovations that have enabled researchers to alleviate the detrimental effects of the strong dipolar couplings between protons, which had led to fast relaxation and broad resonances previously. Particularly proton dilution by deuterons and fast magic-angle spinning (MAS), independently or in a combined way, have been proven to be suitable remedies (Agarwal et al. 2006; Chevelkov et al. 2006; Lewandowski et al. 2011; Linser et al. 2008; Marchetti et al. 2012; Paulson et al. 2003). Accordingly, protons—which have the highest gyromagnetic ratio of all commonly available nuclei in biological NMR—have now become a sensitive and overall highly attractive reporter of molecular structure (Huber et al. 2011; Knight et al. 2012; Linser et al. 2014; Schanda et al. 2009; Zhou et al. 2007), of dynamics (Chevelkov et al. 2007, 2009; Krushelnitsky et al. 2009; Linser et al. 2010a; Ma et al. 2014; Schanda et al. 2010; Zinkevich et al. 2013) and protein interactions (Lamley et al. 2014; Linser et al. 2009; Sinnige et al. 2014; Ward et al. 2011).

Sequential backbone assignment in target proteins is essential for most structural-biology studies based on solid-state NMR spectroscopy. For this purpose, amide protons have proven to be tremendously useful as a complementary element in addition to heteronuclear chemical shifts and as a means to boost the signal to noise per amount of material. Various backbone assignment strategies based on ^{1}H chemical shifts have been proposed, using either scalar couplings or dipolar cross polarization (CP) to elicit

ShengQi Xiang and Kristof Grohe have contributed equally to this work.

Electronic supplementary material The online version of this article (doi:10.1007/s10858-015-9945-4) contains supplementary material, which is available to authorized users.

✉ Rasmus Linser
rali@nmr.mpibpc.mpg.de

[1] Department for NMR-Based Structural Biology, Max Planck Institute for Biophysical Chemistry, Göttingen, Germany

internuclear magnetization transfer. This choice is mostly related to characteristics of the sample—in particular transverse relaxation rates—and the scope of the experiment. Exclusively INEPT- (Morris and Freeman 1979) or TROSY-based approaches (Pervushin et al. 1997) have been shown to be favorable under certain conditions in the solid state. This is the case when relaxation induced by proton dipolar couplings is effectively reduced. Scalar transfers are also applicable to such residues that undergo fast or slow motion (Linser et al. 2008, 2010a). Both, fully CP-based pulse sequences (Chevelkov et al. 2013; Mainz et al. 2013; Xiang et al. 2014; Zhou et al. 2007) and mixed variants with CC–scalar transfers and heteronuclear CPs (Barbet-Massin et al. 2013; Knight et al. 2011; Linser et al. 2011b) have been shown to enable triple-resonance correlations. CC scalar transfers are viable for rigid residues under those experimental conditions for which the ^{13}C transverse relaxation rates T_2 under fast MAS are sufficiently long. The weak scalar couplings, however, limit the scope of scalar transfers in the solid state and provide practical limitations to the range of approaches for assignment and other experiments. In CC INEPT experiments, the involved nuclei are transverse for a time period of approximately 15–25 ms, in which antiphase coherence needs to be evolved and successively be refocused.

If transverse relaxation times T_2 are sufficiently long, the INEPT can deliver a better sensitivity than repeated use of CP with a given maximum efficiency even for rigid residues (Linser et al. 2010a). Also, in out-and-back experiments, scalar couplings can simply be refocused on "the way back" or, as in case of HNCACB-type experiments, evolved and refocused only to half their maximum evolution (Wittekind and Mueller 1993). For experiments with many transfers between different nuclei with small internuclear scalar couplings, however, refocused INEPT can present a significant bottleneck.

In addition to out-and-back sequential backbone assignment experiments, sequential amide-to-amide correlations have long been suggested in solution NMR (Grzesiek et al. 1993; Sun et al. 2005; Weisemann et al. 1993). There they form a complement to ^{13}C-based backbone assignments. In comparison to ^{13}C-based experiments, these provide complementary information, exploit the potentially high amide dispersion, and give rise to a direct and intuitive assignment procedure. However, due to the fact that they are "straight-through" experiments, the INEPT evolution/refocusing period cannot be shortened like in the HNCACB experiment, and consequently they are comparably insensitive and mostly used in solution NMR for proteins of intrinsic disorder (Harbison et al. 2012).

With the possibility of efficient dipolar transfers (Pines et al. 1973), including homonulear ^{13}C–^{13}C CPs, in the solid state (Chevelkov et al. 2013; Nielsen et al. 1994), the main solution-state drawbacks are not encountered for solid proteins, making sequential amide-to-amide correlations an attractive and straightforward means for facilitated resonance assignment. In this work, we demonstrate the usefulness of sequential amide-to-amide correlations and compare their performance with a set of established ^{13}C-edited experiments used for the same purpose, employing the SH3 domain of α-spectrin as a model system.

Materials and methods

Sample preparation

Spectra of the SH3 domain of chicken α-spectrin were recorded using approximately 1–2 mg of uniformly ^{2}H,^{15}N,^{13}C-labelled protein, which was expressed and purified as described earlier (Linser et al. 2007) with additional use of 75 mg α-keto-isovalerate and 125 mg α-ketobutyrate as described previously for solution NMR (Gardner et al. 1997). Micro-crystallization was pursued in a buffer containing 100 % H_2O as well as 75 mM $(NH_4)_2$[Cu(edta)] by pH shift from 3.5 to 7.5. The material was then center-packed into a 1.3 mm rotor using fluorinated rubber plugs in the bottom and top of the rotor.

Solid-state NMR experiments

All NMR experiments were carried out at 800 MHz proton Larmor frequency, 56 kHz MAS, and 35 °C effective temperature, using a 1.3 mm triple-resonance probe on a Bruker Avance III spectrometer.

Here we propose two experiments for amide-to-amide sequential transfers (Fig. 1a, b) that make use of multiple CP steps to transfer magnetization between adjoining amide groups as opposed to *J*-based transfers described in the solution NMR literature. The (H)N(CO)(CA)NH pulse sequence provides inter-residue correlations of $^{1}H_i^N$, $^{15}N_i$ and $^{15}N_{i+1}$ (Fig. 1a, c). The initial magnetization on $^{1}H_{i+1}^N$ is transferred to $^{15}N_{i+1}$ by CP and then further distributed to $^{13}CO_i$ by SPECIFIC-CP (Baldus et al. 1998). Subsequently, the magnetization on $^{13}CO_i$ is transferred to $^{13}CA_i$ using HORROR (Chevelkov et al. 2013; Nielsen et al. 1994), then to $^{15}N_i$ by SPECIFIC-CP, and finally to $^{1}H_i^N$ for detection. The chemical-shift periods are inserted at the position where $^{1}H_i^N$, $^{15}N_i$ and $^{15}N_{i+1}$ magnetization are in the transverse plane. In the middle of each ^{15}N evolution period, a composite 90_x–180_y–90_x carbon pulse centered at 120 ppm is inserted to refocus ^{15}N–^{13}CA and ^{15}N–^{13}CO *J* couplings. $^{1}H^N$–^{15}N *J* couplings are removed by low-power XiX (Ernst et al. 2003) applied on $^{1}H^N$. Waltz-16

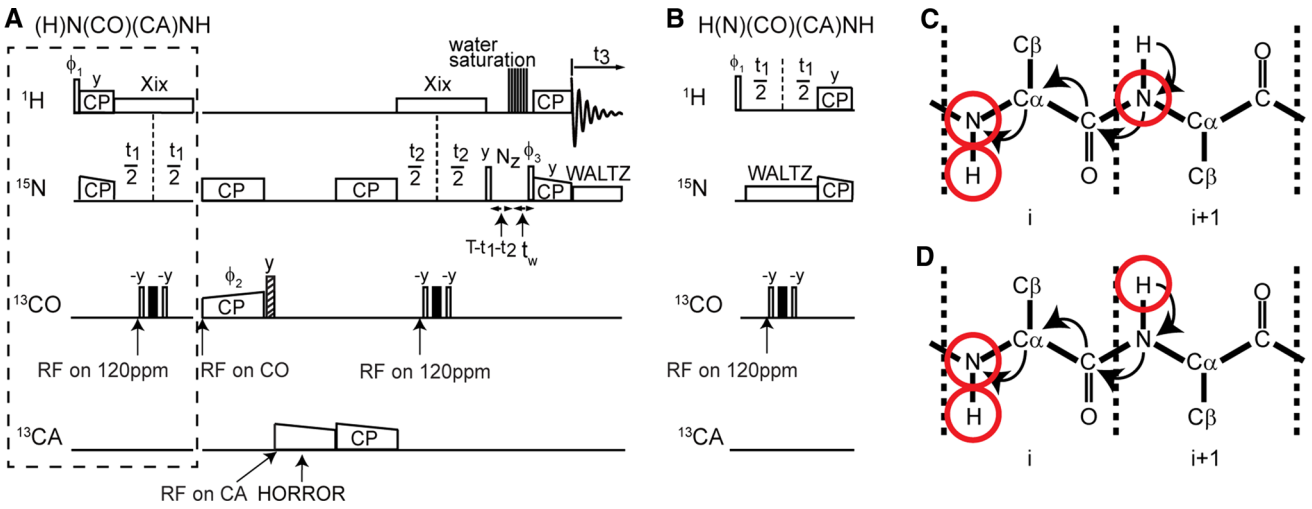

Fig. 1 Magnetization transfer scheme and pulse programs. **a** (H)N(CO)(CA)NH pulse sequence to obtain $^{1}H_{i}^{N}$, $^{15}N_{i}$ and $^{15}N_{i+1}$ correlations. Replacement of the *box* by **b** results in the H(N)(CO)(CA)NH pulse sequence to obtain $^{1}H_{i}^{N}$, $^{15}N_{i}$ and $^{1}H_{i+1}^{N}$ correlations. *Open*, *filled*, and *striped bars* represent 90°, 180°, and trim pulses, respectively. The train of proton pulses for water saturation follows the MISSISSIPI approach (Zhou and Rienstra 2008). All other pulses were applied with phase x if not indicated explicitly. The phase cycle $\phi_1 = x, -x$; $\phi_2 = 4(+x), 4(-x)$; $\phi_3 = x, x, -x, -x$; $\phi_{rec} = x, -x, -x, x, -x, x, x, -x$ was employed. **c**, **d** Schematic representation of the inter-spin correlations and magnetization transfers provided by (H)N(CO)(CA)NH and H(N)(CO)(CA)NH, respectively. The *red circles* represent the chemical shift-encoded nuclei in the two experiments

(Shaka et al. 1983) is applied on ^{15}N during proton detection. A train of proton pulses saturates the water signal when ^{15}N magnetization is along the +z direction before transfer to the adjacent amide proton in accordance with the MISSISSIPPI approach (Zhou and Rienstra 2008).

The H(N)(CO)(CA)NH pulse sequence (Fig. 1b, e), utilizes the same magnetization transfer scheme with minor modifications regarding the evolution period, which now correlates $^{1}H_{i}^{N}$ and $^{15}N_{i}$ with $^{1}H_{i+1}^{N}$. Instead of $^{15}N_{i+1}$, the first evolution period reflects evolution of $^{1}H_{i+1}^{N}$ chemical shift. During this evolution period, Waltz-16 is applied on ^{15}N to remove $^{1}H^{N}$–^{15}N *J* couplings. See the Supplementary Material for maximum acquisition times and apodization.

In the (H)CONH, (H)CO(CA)NH, (H)CANH and (H)CA(CO)NH pulse sequences, $^{1}H^{N}$ magnetization was first transferred to ^{13}CO or ^{13}CA by CP. Transfers between ^{13}CO and ^{13}CA were achieved by use of refocused INEPTs, implemented as described in the literature (Knight et al. 2011; Linser et al. 2008, 2011b; Marchetti et al. 2012), using soft rectangular on-resonance and Gaussian Q3 off-resonance selective ^{13}C pulses (Emsley and Bodenhausen 1990). Magnetization was then transferred to ^{15}N by SPECIFIC-CP, and finally to $^{1}H^{N}$ for detection.

Data processing, chemical-shift assignment, read-out of intensities, and preparation of figures was performed using Bruker Topspin, Cara (Keller 2005), Sparky (Goddard and Kneller 2004), and CcpNmr Analysis software (Vranken et al. 2005), respectively.

For assessment of chemical-shift probabilities of a given nucleus, we added the shift distributions for that nucleus type of each amino-acid type as obtained from the Biological Magnetic Resonance Bank (BMRB) data base (Ulrich et al. 2008). Hereby, we took into account a weighting factor reflecting the abundance of each amino acid type as found in the BMRB statistics. For each nucleus ($^{1}H^{N}$, $^{15}N^{H}$, ^{13}CO, ^{13}CA), the integral of the distribution resulting after summation of the weighted distributions of the individual amino acids (probability per ppm) over the whole chemical shift range was set to 100 %.

Results and discussion

Two amide-to-amide experiments, H(N)(CO)(CA)NH and (H)N(CO)(CA)NH, were recorded to obtain sequential connections between amide groups for perdeuterated proteins under very fast MAS conditions. In the first experiment, $^{1}H_{i}^{N}$, $^{15}N_{i}$ and $^{15}N_{i+1}$ are correlated (Fig. 1a, c), while in the second one $^{1}H_{i}^{N}$ and $^{15}N_{i}$ are correlated to H_{i+1}^{N} (Fig. 1b, d). Each of the two three-dimensional experiments enables a sequential backbone walk, either based on $^{1}H^{N}$ or on ^{15}N chemical shifts. The separation of sequential strips in the second and third dimension is given by the amide ^{1}H and ^{15}N dispersion of the protein.

Overall, 50 out of 60 non-proline residues were observed in the two amide-to-amide spectra. Peaks of eight residues, located in stretches 1–6 and 47–48, are absent due

to their high mobility, which is consistent with previous studies on the same protein (Linser et al. 2008; van Rossum et al. 2003). Accordingly, these residues are also missing in dipolar-transfer-based 2D (H)NH or 3D (H)CANH/(H)CONH spectra. The peaks of residues 37 and 38 are at the noise level in all 3D experiments. The last residue, D62, is absent in sequential amide-to-amide spectra because of its missing neighbor.

The backbone walk is illustrated in Fig. 2a, b and depicts strips from L12 to S19. The two different experiments provide complementary information. The intraresidual-correlation complement in each spectrum ($^{1}H_i$,$^{15}N_i$,$^{1}H_i$ and $^{15}N_i$,$^{15}N_i$,$^{1}H_i$, respectively) is automatically given by the diagonal of each strip and hence unnecessary to acquire separately. There is no interresidual correlation peak in the strips of S19 since the 20th residue is a proline.

In order to assess the performance of the sequential amide-to-amide experiments, we compared signal to noise and peak dispersion in these experiments with those that one would expect in commonly employed ^{13}C-based triple-resonance sequential backbone assignment experiments. The first FIDs of 2D (H)NH, 3D (H)CANH, 3D(H)CA(CO)NH and 3D (H)N(CO)(CA)NH are compared in Fig. 3. The first FID of an (H)N(CO)(CA)NH exhibits

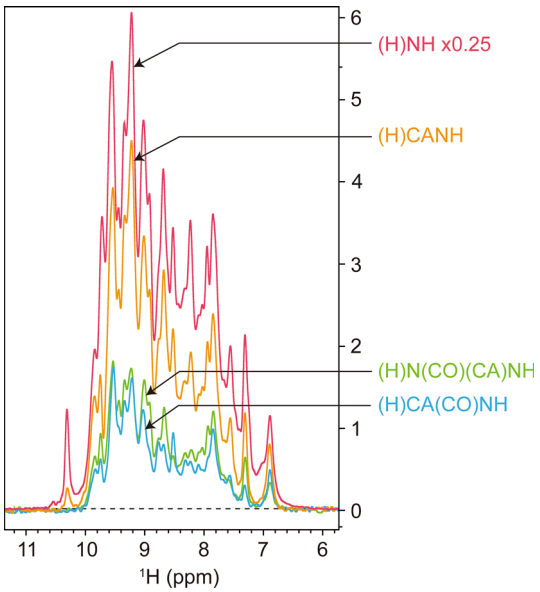

Fig. 3 First FID of different 2D and 3D experiments obtained on the same SH3 sample with the same number of scans. (H)NH, (H)CANH, (H)N(CO)(CA)NH and (H)CA(CO)NH are drawn with *red*, *orange*, *green* and *blue colors*, respectively. The first FID of (H)NH is scaled down to 25 %. (H)CA(CO)NH is recorded with an INEPT ^{13}CA–^{13}CO transfer

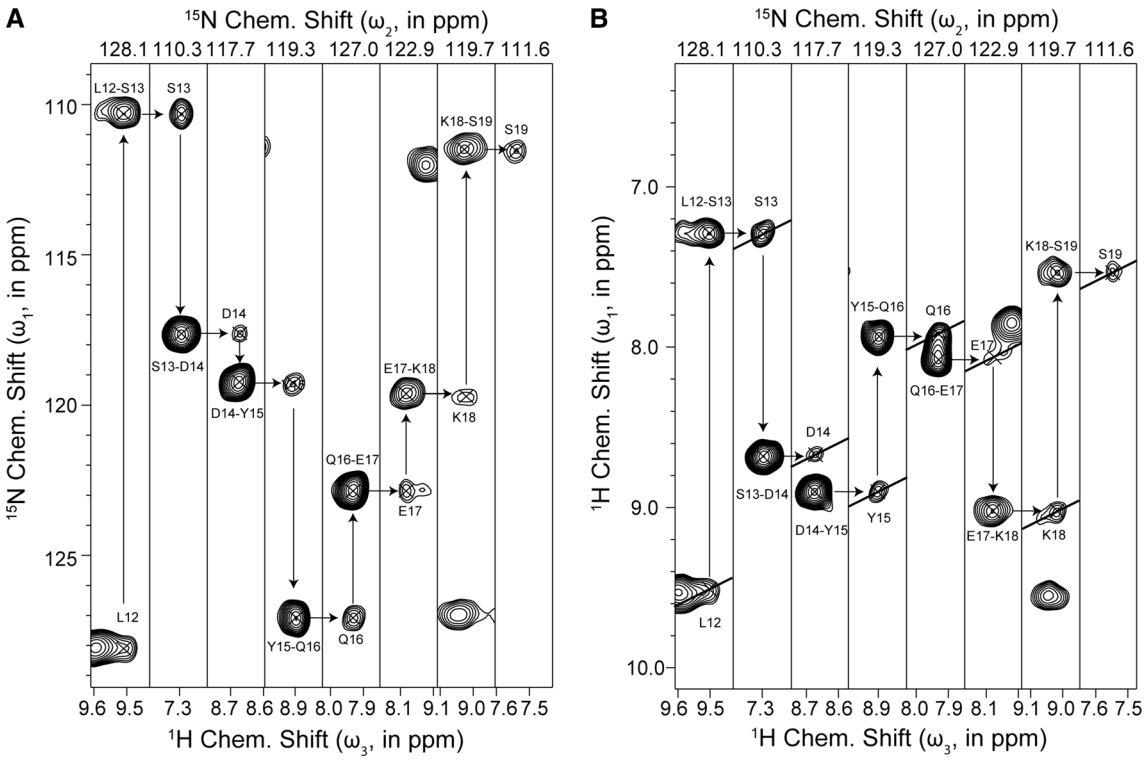

Fig. 2 Strips from (H)N(CO)(CA)NH (**a**) and H(N)(CO)(CA)NH (**b**) spectra illustrate the unambiguous sequential backbone walks between residue L12 and S19. The 20th residue is a proline. The *residue numbers in their labels* indicate autocorrelation and inter-residual correlation peaks. The *arrows* show individual steps of the walk. The *black lines* crossing autocorrelation peaks highlight the *diagonal lines* of each ^{1}H–^{1}H 2D plane

~7 % intensity of the signal in a (H)NH spectra. Although (H)N(CO)(CA)NH uses more transfer steps than (H)CA(CO)NH does, its first FID is slightly stronger. (The first FID of an (H)CO(CA)NH bears similar (slightly weaker) signal to noise as the (H)CA(CO)NH under identical conditions in our hands, see the Supplementary Material, Figure S3.) As shown in the spectra in Fig. 2, there are weak (redundant) autocorrelation peaks in both amide-to-amide spectra. On average, the intensities of the autocorrelation peaks are 27 % of the intensities of inter-residue peaks, which means that 21 % of total ^{13}C magnetization is transferred back to the starting point. This is supposedly due to incomplete CC transfer or potential two-bond NC transfer. Even taking this incomplete transfer into account, the sequential transfer efficiency of amide-to-amide experiments is similar to that of (H)CA(CO)NH/(H)CO(CA)NH. A detailed analysis of residue-resolved signal-to-noise ratios in the different spectra (Fig. S1) proves that amide-to-amide spectra are more sensitive than, or at least comparable to (H)CA(CO)NH or (H)CO(CA)NH spectra for the SH3 domain. Despite a lower number of transfer steps, the relatively long duration of the refocused INEPT transfer between ^{13}CA and ^{13}CO is a potential source for loss of magnetization in the scalar experiments. In addition, during indirect evolutions of ^{13}CA and ^{13}CO, the carbon band-selective shaped pulses used for removing ^{13}CA–^{13}CO *J* coupling and compensating phase drifts may cause extra signal loss. The low intensities of autocorrelation peaks in amide-to-amide spectra are irrelevant for the assignment procedure because the positions of autocorrelation peaks are trivial and not needed in the backbone walk as discussed above. The sensitivity of the sequential amide-to-amide experiments may thus be at least as high or potentially higher than the weaker required experiments of the common ^{13}C-based experiment pairs.

The $^{1}H^{N}$-encoded experiment can alternatively be conducted using a direct $^{1}H^{N}/^{13}CO$ CP initially to increase the signal to noise. This, however, would sacrifice part of the specificity, since a back-transfer to the distant ^{13}CO is theoretically possible as well and also other through-space transfers may arise (Linser 2012). All experiments can alternatively be acquired equally well in an inverted order to correlate residues in the other direction, e.g. as an (H)N(CA)(CO)NH etc.

When used in addition to the ^{13}C evolution-based experiments, which utilize $^{13}CA/^{13}CO$ chemical shifts to provide backbone assignments, the amide-to-amide experiments provide complementary information from amide shifts, which reduces the ambiguity of sequential connections and thus facilitates the assignment procedure. In addition, the chemical shift values of the amide group, especially the ^{15}N chemical shifts, have broader and more even distributions in units of observed line widths for perdeuterated samples under very fast MAS conditions. For example, in the current 3D experiments on the SH3 domain, ^{15}N chemical shifts cover 23.4 ppm, and the average line width of ^{15}N is 0.96 ppm. This means that the ^{15}N chemical shifts are spread over more than 24 times their line width. By contrast, ^{13}CO chemical shifts values are only spread over 12.5 times their average line-width. Therefore, the peaks in the ^{15}N dimension tends to be less crowded. As demonstrated in Fig. 4, there is less ambiguity in searching sequential connections by matching ^{15}N chemical-shift values compared to other backbone nuclei. The ^{1}H shift-modulated H(N)(CO)(CA)NH experiment provides lower resolution than the ^{15}N-modulated counterpart, but it bears comparably high assignment fidelity with respect to the (H)CANH/(H)CA(CO)NH pair. Moreover, the ^{13}C-derived backbone assignment procedure requires comparing chemical shifts from two different spectra, while the amide-to-amide approach looks for matching of chemical shifts in the same spectrum. This further reduces systematic error due to instrument instability and variations in sample conditions.

In the previous section, we considered a single (SH3) protein for assessing ambiguity probabilities. To evaluate the performance of amide-to-amide experiments in terms of resolution under more general conditions, we were interested in the chemical shift distribution of ^{13}CA, ^{13}CO, $^{1}H^{N}$ and ^{15}N signals in the BMRB (considering only diamagnetic systems). When related to the linewidths of the signals, this shift distribution expresses how crowded a spectrum will be in this dimension (see Fig. 5). For each of the 20 proteinogenic amino acids, the average chemical shift of the relevant nuclei and their standard deviations were extracted from the BMRB. Each individual distribution was weighted with the abundance of its amino acid (as obtained from the BMRB) and all distributions for an identical nucleus type added together. The integral of each sum function (for $^{1}H^{N}$, $^{15}N^{H}$, $^{13}C^{\alpha}$, and ^{13}CO) over the whole range of chemical shifts in ppm was then normalized to 100 %. Successively, these distributions as a function of chemical shift in ppm representing the relative number of peaks within one ppm were transformed into curves that quantify the relative number of shifts lying within a range of one linewidth. This substitution corresponds to a nucleus-type-specific scaling of the ppm-based probability values in the Y dimension based on the individual linewidth (in ppm) obtained for this nucleus. Moreover, the space over which the shifts are distributed (one-dimensional spectral space, on the X-axis) was expressed in units of linewidths instead of ppm. This brings the scaled distributions back to an identical area of 100 % when integrated over the total spectral space available in this dimension. The curves are plotted here with the linewidth

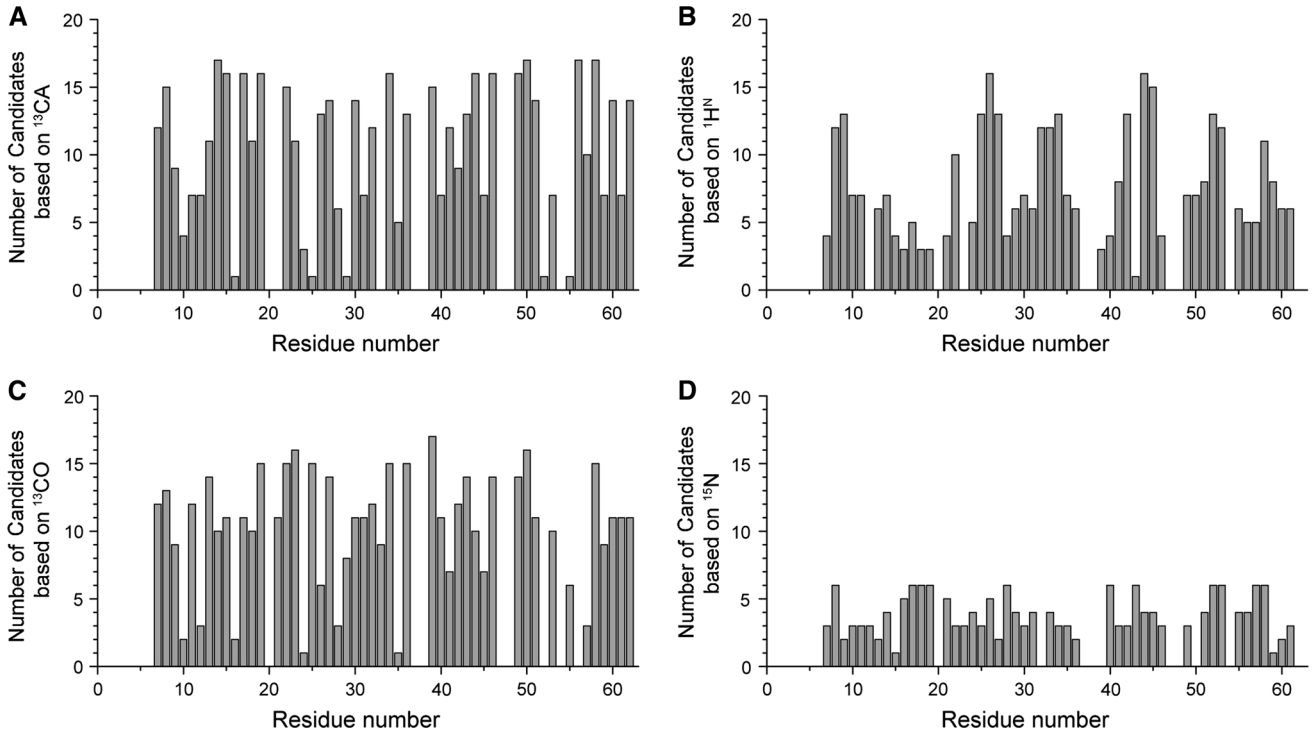

Fig. 4 The number of possible sequential connectivities in the search for matching strips as a function of residue number, based on the experimental chemical shifts in the SH3 domain. **a** For ^{13}CA, **b** for $^{1}H^{N}$, **c** for ^{13}CO and **d** for ^{15}N. The cutoff values in the search for sequential connectivities are set to the observed line width of each nucleus as obtained in our 3D experiments: 0.89 ppm (179 Hz) for ^{13}CA, 0.66 ppm (133 Hz) for ^{13}CO, 0.199 ppm (159 Hz) for ^{1}H and 0.96 ppm (78 Hz) for ^{15}N. Residues 37–38, 47–48, and the first six residues are not included here since they are not observable in 3D spectra

as obtained from indirect dimensions in 3D experiments, representing linewidths of practical relevance. For plots with minimum obtainable linewidths of this protein (natural linewidths with no apodization and truncation) at 800 MHz proton Larmor frequency, the curves were plotted again in the Supplementary Material, Figure S2. The "in-praxis" linewidths above are taken as obtained in our 3D experiments (see the Supplementary Material for a table of maximum acquisition times and apodization), whereas the values for natural linewidths are derived from peaks observed in HSQC spectra with sufficiently long indirect acquisition periods ($^{1}H^{N}$, ^{15}N) without apodization and as described in the literature previously for the same sample under comparable conditions (^{13}C) (Linser et al. 2010b).

Of all four nuclei, the ^{15}N remains the species with least crowdedness (with a maximum probability of 6 % to find a second peak within the range of one line-width of a given shift value, which would happen at around 120 ppm). ^{13}CO is the second best in terms of least overlapping probability (6.5 % chance for a second peak within one line width, if the first one has a shift of 172 ppm) using line widths commonly found in 3D experiments. CO is better than ^{15}N when providing acquisition times allowing for natural linewidths without any truncation. However, to do backbone assignment with ^{13}CO chemical shifts, the (H)CO(CA)NH is required. As shown above, the overall sensitivity of the (H)CO(CA)NH/(H)CONH pair per total time is less than the (H)N(CO)(CA)NH, which indeed makes (H)N(CO)(CA)NH superior to the (H)CO(CA)NH/(H)CONH pair in backbone assignments. The CA linewidth is usually dominated by scalar couplings that are difficult to avoid and bears less resolution. This general problem is reflected in the value of the ^{13}CA plot for the minimal-obtainable linewidth in the Supplementary Material, Figure S2. Whereas the ^{1}H resolution is also dependent on the spinning and deuteration and can have very different feasibility, the ^{15}N linewidth is less prone to be affected by proton dipolar couplings, thus particularly the (H)N(CO)(CA)NH will be of significance to assign fully protonated proteins in future studies. Further increase in resolution can be achieved by running the experiment as a 4D HN(CO)(CA)NH (see the Supplementary Material, Figure S4), which can be implemented in a straightforward way from the 3D pulse programs without further pulse sequence elements (and related sensitivity losses). This can be done for example using Non-Uniform Sampling approaches as we described previously (Hyberts et al. 2012; Linser et al. 2014). In theory, amide backbone assignment can be achieved purely on either of these experiments after

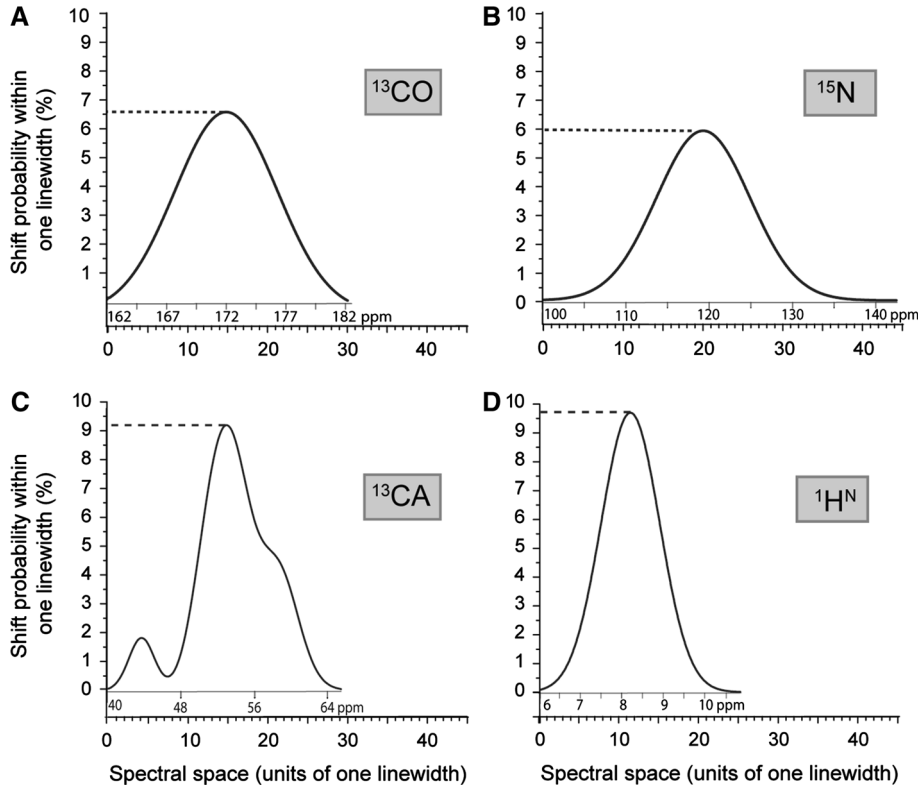

Fig. 5 BMRB data bank distributions of chemical shifts (in %) over the spectral space (in units of one linewidth, FWHM) for ^{13}CO (**a**), ^{15}N (**b**), ^{13}CA (**c**), and ^{1}H^{N} (**d**) dimensions. The *Y-axis values* represent the relative number of signals that fall into a range of one linewidth (i.e., the density of peaks) at each position of the X-axis. The spectral space (X-axis) is represented in units of one linewidth of the individual nucleus (*lower scale*) for consistency. The distributions in **a**–**d** are plotted with identical X-axis dimensions, representing a total width of 45 FWHM, whereas the zero-point is arbitrarily set to the left end of the chemical shift ranges. Necessarily, the integral of the probability of a shift per one linewidth (Y-axis) over the entire spectral space (X-axis in units of linewidth) equals 100 %. For a more practical context, the X-axis scales are translated into units of one ppm of the respective nucleus in each case, which then provides the distribution more intuitively as a function of chemical shift (*upper scale* in *gray*). The height of the curve demonstrates the risk of peaks to fall into the same range (to overlap), so the highest point of each curve is most relevant for comparing the expected risk of shift degeneracy associated with the different nuclei. Shift probabilities were used as obtained from the BMRB database as described in the text. We assumed conservative linewidths of 150 Hz for CO, 160 Hz for ^{13}CA, 150 Hz for ^{15}N, and 150 Hz for ^{1}H^{N}. These values represent linewidths practically obtained in indirect dimensions of standard 3D experiments. See the Supplementary Material for a similar plot assuming minimally obtainable linewidths

HN 2D spectra have been acquired. In praxis, due to their complementarity to ^{13}C-based approaches, the sequential amide-to-amide correlations will be of particular value for proteins in which either tactic alone is not sufficient for unambiguous sequential assignment.

Conclusion

In summary, we have developed a set of amide-to-amide experiments for sequential backbone assignment with low ambiguity and competitive sensitivity compared with ^{13}C-based sequential assignment. The pulse programs were tested using a minimal amount of protein, uniformly ^{2}H,^{15}N,^{13}C-labelled and 100 % $^{1}H_2O$ back-exchanged SH3 domain, at a spin rate of 56 kHz. The two pulse programs can potentially be combined into one single 4D H^{N}N–H^{N}N correlation without the accommodation of further transfer steps. Because of the high sensitivity and broad chemical shift distribution of the amide groups, the described method will be of general use in solid-state NMR studies of larger and more complicated systems.

Acknowledgments R.L. acknowledges support from the Max-Planck Gesellschaft and the Fonds der Chemischen Industrie (FCI) in terms of a Liebig junior group fellowship. R.L. and S.X. acknowledge funding from the DFG Collaborative Research Center 803 (Project A4).

References

Agarwal V, Diehl A, Skrynnikov N, Reif B (2006) High resolution 1H detected 1H, 13C correlation spectra in MAS solid-state NMR using deuterated proteins with selective 1H, 2H isotopic labeling of methyl groups. J Am Chem Soc 128:12620–12621

Agarwal V et al (2014) De novo 3D structure determination from sub-milligram protein samples by solid-state 100 kHz MAS NMR spectroscopy. Angew Chem Int Ed 53:12253–12256

Baldus M, Petkova AT, Herzfeld J, Griffin RG (1998) Cross polarization in the tilted frame: assignment and spectral simplification in heteronuclear spin systems. Mol Phys 95:1197–1207

Barbet-Massin E et al (2013) Out-and-back 13C–13C scalar transfers in protein resonance assignment by proton-detected solid-state NMR under ultra-fast MAS. J Biomol NMR 56:379–386

Barbet-Massin E et al (2014) Rapid proton-detected NMR assignment for proteins with fast magic angle spinning. J Am Chem Soc 136:12489–12497

Bellstedt P, Herbst C, Häfner S, Leppert J, Görlach M, Ramachandran R (2012) Solid state NMR of proteins at high MAS frequencies: symmetry-based mixing and simultaneous acquisition of chemical shift correlation spectra. J Biomol NMR 54:325–335

Brown SP (2012) Applications of high-resolution 1H solid-state NMR. Solid State Nucl Magn Reson 41:1–27

Chevelkov V, Rehbein K, Diel A, Reif B (2006) Ultra-high resolution in proton solid-state NMR spectroscopy at high levels of deuteration. Angew Chem Int Ed 45:3878–3881

Chevelkov V, Faelber K, Schrey A, Rehbein K, Diehl A, Reif B (2007) Differential line broadening in MAS solid-state NMR due to dynamic interference. J Am Chem Soc 129:10195–10200

Chevelkov V, Fink U, Reif B (2009) Accurate determination of order parameters from 1H, 15N dipolar couplings in MAS solid-state NMR experiments. J Am Chem Soc 131:14018–14022

Chevelkov V, Giller K, Becker S, Lange A (2013) Efficient CO–CA transfer in highly deuterated proteins by band-selective homonuclear cross-polarization. J Magn Reson 230:205–211

Emsley L, Bodenhausen G (1990) Gaussian pulse cascades: new analytical functions for rectangular selective inversion and in-phase excitation in NMR. Chem Phys Lett 165:469–476

Ernst M, Samoson A, Meier BH (2003) Low-power XiX decoupling in MAS NMR experiments. J Magn Reson 163:332–339

Gardner KH, Rosen MK, Kay LE (1997) Global folds of highly deuterated, methyl-protonated proteins by multidimensional NMR. Biochemistry 36:1389–1401

Goddard TD, Kneller DG (2004) SPARKY 3. University of California, San Francisco

Grzesiek S, Anglister J, Ren H, Bax A (1993) ^{13}C line narrowing by deuterium decoupling in ^{2}D/^{13}C/^{15}N enriched proteins. Application to triple resonance 4D J connectivity of sequential amides. J Am Chem Soc 115:4369–4370

Harbison NW, Bhattacharya S, Eliezer D (2012) Assigning backbone NMR resonances for full length tau isoforms: efficient compromise between manual assignments and reduced dimensionality. PLoS One. doi:10.1371/journal.pone.0034679

Huber M, Hiller S, Schanda P, Ernst M, Böckmann A, Verel R, Meier BH (2011) A proton-detected 4D solid-state NMR experiment for protein structure determination. ChemPhysChem 12:915–918

Hyberts SG, Milbradt AG, Wagner AB, Arthanari H, Wagner G (2012) Application of iterative soft thresholding for fast reconstruction of NMR data non-uniformly sampled with multidimensional poisson gap scheduling. J Biomol NMR 52:315–327

Keller RLJ (2005) Optimizing the process of nuclear magnetic resonance spectrum analysis and computer aided resonance assignment. Doctoral and habilitation theses ETH

Knight MJ et al (2011) Fast resonance assignment and fold determination of human superoxide dismutase by high-resolution proton-detected solid-state MAS NMR spectroscopy. Angew Chem Int Ed 50:11697–11701

Knight MJ et al (2012) Structure and backbone dynamics of a microcrystalline metalloprotein by solid-state NMR. Proc Natl Acad Sci USA 109:11095–11100

Krushelnitsky A, deAzevedo E, Linser R, Reif B, Saalwächter K, Reichert D (2009) Direct observation of millisecond to second motions in proteins by dipolar CODEX NMR spectroscopy. J Am Chem Soc 131:12097–12099

Lamley JM et al (2014) Solid-state NMR of a protein in a precipitated complex with a full-length antibody. J Am Chem Soc 136:16800–16806

Lewandowski JR, Dumez J-N, Akbey U, Lange S, Emsley L, Oschkinat H (2011) Enhanced resolution and coherence lifetimes in the solid-state NMR spectroscopy of perdeuterated proteins under ultrafast magic-angle spinning. J Phys Chem Lett 2:2205–2211

Linser R (2012) Backbone assignment of perdeuterated proteins using long-range H/C-dipolar transfers. J Biomol NMR 52:151–158

Linser R, Chevelkov V, Diehl A, Reif B (2007) Sensitivity enhancement using paramagnetic relaxation in MAS solid-state NMR of perdeuterated proteins. J Magn Reson 189:209–216

Linser R, Fink U, Reif B (2008) Proton-detected scalar coupling based assignment strategies in MAS solid-state NMR spectroscopy applied to perdeuterated proteins. J Magn Reson 193:89–93

Linser R, Fink U, Reif B (2009) Probing surface accessibility of proteins using paramagnetic relaxation in solid-state NMR spectroscopy. J Am Chem Soc 131:13703–13708

Linser R, Fink U, Reif B (2010a) Assignment of dynamic regions in biological solids enabled by spin-state selective NMR experiments. J Am Chem Soc 132:8891–8893

Linser R, Fink U, Reif B (2010b) Narrow carbonyl resonances in proton-diluted proteins facilitate NMR assignments in the solid state. J Biomol NMR 47:1–6

Linser R, Bardiaux B, Higman V, Fink U, Reif B (2011a) Structure calculation from unambiguous long-range amide and methyl 1H–1H distance restraints for a micro-crystalline protein with MAS solid state NMR. J Am Chem Soc 133:5905–5912

Linser R et al (2011b) Proton detected solid-state NMR of fibrillar and membrane proteins. Angew Chem Int Ed 50:4508–4512

Linser R, Bardiaux B, Hyberts SG, Kwan AH, Morris VK, Sunde M, Wagner G (2014) Solid-state NMR structure determination from diagonal-compensated, sparsely nonuniform-sampled 4D proton–proton restraints. J Am Chem Soc 136:11002–11010

Ma P et al (2014) Probing transient conformational states of proteins by solid-state R(1ρ) relaxation-dispersion NMR spectroscopy. Angew Chem Int Ed 53:4312–4317

Mainz A, Religa T, Sprangers R, Linser R, Kay LE, Reif B (2013) Solution-state NMR spectroscopy at 1 MDa and beyond. Angew Chem Int Ed 52:8746–8751

Marchetti A et al (2012) Backbone assignment of fully protonated solid proteins by 1H detection and ultrafast magic-angle-spinning NMR spectroscopy. Angew Chem Int Ed 51:10756–10759

Morris GA, Freeman R (1979) Enhancement of nuclear magnetic resonance signals by polarization transfer. J Am Chem Soc 101:760–762

Nielsen NC, Bildsoe H, Jakobsen HJ, Levitt MH (1994) Double-quantum homonuclear rotary resonance: efficient dipolar recovery in magic-angle spinning nuclear magnetic resonance. J Chem Phys 101:1805–1812

Nishiyama Y, Malon M, Ishii Y, Ramamoorthy A (2014) 3D 15N/15N/1H chemical shift correlation experiment utilizing an RFDR-based 1H/1H mixing period at 100 kHz MAS. J Magn Reson 244:1–5

Paulson EK, Morcombe CR, Gaponenko V, Dancheck B, Byrd RA, Zilm KW (2003) Sensitive high resolution inverse detection NMR spectroscopy of proteins in the solid state. J Am Chem Soc 125:15831–15836

Pervushin KV, Riek R, Wider G, Wüthrich K (1997) Attenuated T2 relaxation by mutual cancellation of dipole–dipole coupling and

chemical shift anisotropy indicates an avenue to NMR structures of very large biological macromolecules. Proc Natl Acad Sci USA 94:12366–12371

Pines A, Gibby MG, Waugh JS (1973) Proton-enhanced NMR of dilute spins in solids. J Chem Phys 59(2):569–590

Schanda P, Huber M, Verel R, Ernst M, Meier BH (2009) Direct detection of $^{3h}J_{NC'}$ hydrogen-bond scalar couplings in proteins by solid-state NMR spectroscopy. Angew Chem Int Ed 48:9322–9325

Schanda P, Meier BH, Ernst M (2010) Quantitative analysis of protein backbone dynamics in microcrystalline ubiquitin by solid-state NMR spectroscopy. J Am Chem Soc 132:15957–15967

Shaka AJ, Keeler J, Frenkiel T, Freeman R (1983) An improved sequence for broad-band decoupling—WALTZ-16. J Magn Reson 52:335–338

Sinnige T, Daniëls M, Baldus M, Weingarth M (2014) Proton clouds to measure long-range contacts between nonexchangeable side chain protons in solid-state NMR. J Am Chem Soc 136:4452–4455

Sun Z-Y, Frueh D, Selenko P, Hoch J, Wagner G (2005) Fast assignment of 15N-HSQC peaks using high-resolution 3D HNcocaNH experiments with non-uniform sampling. J Biomol NMR 33:43–50

Ulrich EL et al (2008) BioMagResBank. Nucleic Acids Res 36:D402–D408

van Rossum BJ, Castellani F, Pauli J, Rehbein K, Hollander J, de Groot HJM, Oschkinat H (2003) Assignment of amide proton signals by combined evaluation of HN, NN and HNCA MAS–NMR correlation spectra. J Biomol NMR 25:217–223

Vranken WF et al (2005) The CCPN data model for NMR spectroscopy: development of a software pipeline. Proteins 59:687–696

Ward ME, Shi L, Lake E, Krishnamurthy S, Hutchins H, Brown LS, Ladizhansky V (2011) Proton-detected solid-state NMR reveals intramembrane polar networks in a seven-helical transmembrane protein proteorhodopsin. J Am Chem Soc 133:17434–17443

Weisemann R, Rüterjans H, Bermel W (1993) 3D triple-resonance NMR techniques for the sequential assignment of NH and 15N resonances in 15N- and 13C-labelled proteins. J Biomol NMR 3:113–120

Wittekind M, Mueller L (1993) HNCACB: a high sensitivity 3D NMR experiment to correlate amide proton and nitrogen resonances with the α-carbon and β-carbon resonances in proteins. J Magn Reson B 101:201–205

Xiang S, Chevelkov V, Becker S, Lange A (2014) Towards automatic protein backbone assignment using proton-detected 4D solid-state NMR data. J Biomol NMR 60:85–90

Zhou DH, Rienstra CM (2008) High-performance solvent suppression for proton-detected solid-state NMR. J Magn Reson 192:167–172

Zhou DH et al (2007) Solid-state protein structure determination with proton-detected triple resonance 3D magic-angle spinning NMR spectroscopy. Angew Chem Int Ed 46:8380–8383

Zhou DH et al (2012) Solid-state NMR analysis of membrane proteins and protein aggregates by proton detected spectroscopy. J Magn Reson 54:291–305

Zinkevich T, Chevelkov V, Reif B, Saalwächter K, Krushelnitsky A (2013) Internal protein dynamics on ps to μs timescales as studied by multi-frequency 15N solid-state NMR relaxation. J Biomol NMR 57:219–235